Article

Development of Multi-part Field-Shapers for Magnetic-Pulse Welding Using Nanostructured Cu-Nb Composite

Evgeny Zaytsev *, Vasiliy Krutikov, Alexey Spirin, Sergey Paranin

Posted Date: 26 March 2024

doi: 10.20944/preprints202403.1582.v1

Keywords: magnetic pulse welding; field-shaper; nanostructured Cu-Nb composite

 doi:10.20944/preprints202403.1582.v1

Article

Development of Multi-Part Field-Shapers for Magnetic-Pulse Welding Using Nanostructured Cu-Nb Composite

Evgeny Zaytsev [1,*], Krutikov Vasiliy [1], Alexey Spirin [1] and Sergey Paranin [1]

Institute of Electrophysics of the Ural Branch of the Russian Academy of Sciences, 620016, 106 Amundsen str., Yekaterinburg, Russia

* Correspondence: jzaizew@gmail.com

Abstract: Magnetic pulse welding (MPW) employs high pulsed magnetic field to accelerate parts against each other thus forming an impact joining. Single-turn tool coils and field-shapers (FS) used in MPW operate under the most demanding conditions: a magnetic field of 40-50 T with a period of tens of microseconds. For conventional copper and bronze coils intense thermo-mechanical stresses lead to rapid degradation of the working bore. This work is aimed to improve the efficiency of field-shapers and focused on development of 2- and 4-slit FS with nanocomposite Cu 18Nb wire brazed as FS inner current-carrying layer. The measured ratio of magnetic field to discharge current was 56.3 and 50.6 T/MA for 2- and 4-slit FS respectively. FEM calculations of magnetic field generation showed its 6-9% and 3% variation for 2- and 4-slit FS respectively. The results of copper tube compression have shown an ovality of 27% and 7% for 2- and 4-slit FS respectively. The measured deviation of weld joining length was 11% and 1.4% in 2- and 4-slit FS respectively. Compared to the previous experiments on the whole steel inductor, the novel FS showed significantly better results in terms of efficiency and homogeneity of the magnetic field.

Keywords: magnetic pulse welding; field-shaper; nanostructured Cu-Nb composite

1. Introduction

One of the main applications of high pulsed magnetic fields (HMF) of 10–100 microseconds duration is magnetic pulse processing of metals. These technologies provide promising results in metals forming ang welding, as well as compaction of nanopowders inside conductive shells [1,2]. The main tool for generating magnetic fields is a single- or multi-turn coil or inductor, often with field-shapers (FS). The highest requirements to the field pulse are imposed by the process of magnetic pulse welding (MPW), especially for high-strength, hard-to-weld steels, *e.g.*, ferritic-martensitic steels for nuclear industry [3–5], where a field of 40–50 T is generated in the inductor at 10–20 μs half-period. The energy of the magnetic field is transferred to the kinetic energy of the metal workpiece, which leads to the collision of the welding parts at speeds of 300–500 m/s, and forming metallurgical bonds.

Apart from the process of material joining itself, the actual aim of MPW research is to increase the inductor efficiency and lifetime. For example, the conventional copper and bronze (CuBe2) inductors are not capable of repetitive (at least several hundred pulses per lifetime) generation of such fields [6–8]. Intensive thermomechanical stresses, especially Joule heating, in the surface layer of the inductor lead to the formation of cracks and its further destruction [9,10]. Strong materials, such as steels, can be used for inductors to increase the durability, however, this leads to another issues: higher resistivity of steels causes the discharge current to increase, which reduces the lifetime of the coil, and this higher resistivity reduces the azimuthal homogeneity of the magnetic field. Circumferential drops in the magnetic field near the gaps in the field-shaper affect the quality of the welded joint.

Nanostructured Cu-Nb alloy has proven to be the most promising material for high field inductor construction. It became possible due to the combination of high conductivity (50-70% IACS) and outstandingly high strength (ultimate tensile strength up to 1500 MPa) [11–13] . Those properties are achieved due to the fiber structure (niobium fibers with diameter ∼100 nm is distributed in the copper matrix) obtained in the accumulative drawing and bundling (ADB) process [13–15]. Thus, multifold

 doi:10.20944/preprints202403.1582.v1

generation of fields with amplitudes up to 45 T [16], 72 T [17], 90 T [18], 100 T [19–21] and duration dozens-hundreds of milliseconds were obtained in multi-turn coils made of this material. However, due to fundamental differences in the design of multi- and single-turn inductors that complicate the use of fiber composite, there are no works devoted to the development and study of this material for the generation of shorter magnetic field pulses.

The aim of this work was to improve the existing MPW single-turn inductor design in order to improve its performance, in particular, to increase magnetic field circumferential (azimuthal) uniformity and enhance energy efficiency, i.e. increase B_m / I_m ratio. The main approach in the present work is the use of the abovementioned Cu-Nb composite wire to upgrade the steel inductors that worked previously. For more comprehensive study, FEM modeling of the developed systems was carried out using Ansys Maxwell 3D.

2. Basics of MPW Process and the Role of Field-Shaper

The MPW setup (Figure 1) consists of pulse current generator (PCG) which is loaded to a coil with a field-shaper and a workpiece inside (Figure 1a). Once the capacitor bank is charged to the required energy, it is switched to the coil by triggered vacuum switches. The discharge current form magnetic field in the working bore (channel) of the inductor, which induces eddy currents in the field-shaper and the workpiece (Figure 1b). The Lorentz force (F_L) from the interaction of the magnetic field with the induced currents makes pressures up to 2 GPa (70 T) on the workpiece, which makes it possible to perform its radial compression with hundreds of m/s velocities. To observe a high-quality joint, it is necessary that the impact velocity V_i and the contact point velocity V_c (Figure 1c) were within a certain range of values, known in the literature as the welding window [22–24].

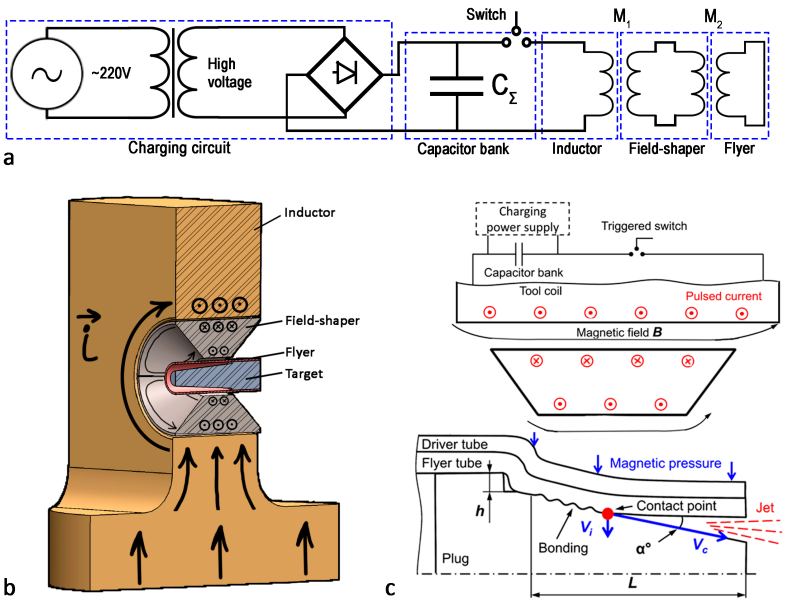

Figure 1. MPW setup schematic: electrical schematic (**a**), single-turn inductor with FS (**b**), joining geometry (**c**)

Radial compression of a cylindrical conducting tube in one dimensional (axisymmetric) model can be described by the following equation:

$$\ddot{r} = \frac{S}{m}(P_m - P_t), \tag{1}$$

where S/m is the specific area of the tube, $\ddot{r}$ is the radial acceleration of the middle of the tube wall, P_t is the pressure required for the occurrence of plastic deformations of the tube, $P_m = B^2/2\mu_0$ is the pressure of the magnetic field created by the discharge current with frequency ω:

 doi:10.20944/preprints202403.1582.v1

$$B(t) = B_m \sin \omega t \tag{2}$$

In order to describe the radial compression velocity, it is necessary to integrate equation (1) over time (from the initial moment of discharge $t = 0$, to the moment of tube-plug collision $t = t_{end}$):

$$\dot{r} = \int_0^{t_{end}} \frac{S}{m} \left(\frac{B(t)^2}{2\mu_0} - P_t \right) dt \tag{3}$$

This equation shows that the velocity of the tube wall is proportional to the square of the magnetic induction B. In the case of a real inductor system, the magnetic field pressure at different points on the surface may differ. Thus, a 10% difference in the magnetic field induction will lead to an approximately 20% difference in the radial velocity.

Accordingly, the optimization of inductor system design to increase the magnetic field homogeneity on the surface of the workpiece is one of the most urgent tasks. The magnetic field has drops near gaps in field-shaper, so a common approach to smooth azimuthal magnetic field distribution is to increase the number of gaps or slits in FS (Figure 2). This approach is practiced for both planar and cylindrical geometries [25,26]. Four slits, according to these works, was found optimal, which was confirmed by experiment. The position of the FS in the inductor also affects the homogeneity of the magnetic field. Thus, in the work of Shen's team it was shown that the most uniform compression of aluminum alloy tube was achieved when the angle between the plane of the FS slit and the plane of the inductor slit was 90° [27].

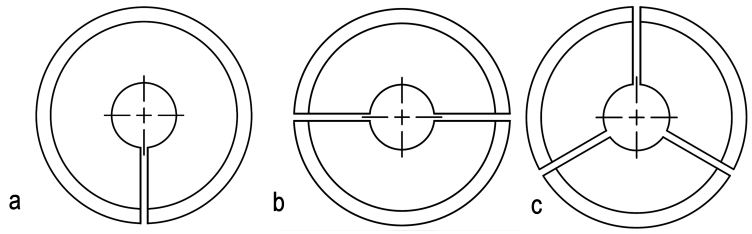

Figure 2. Field-shaper for cylindrical geometry with different number of slits (1 (**a**), 2 (**b**), 3 (**c**))

Another task is a general increase in pulsed magnetic field generation efficiency and homogeneity related to the FS geometry. Thus, to solve this problem, it is possible to change the FS cross section. Rajak and colleagues investigated the stepped (Figure 3a) and tapered (Figure 3b) FS cross-sectional profile [28,29]. The work has shown that single-stepped profile gives the best peak field B_m for the same charging energy, however using a stepped design reduces its overall stiffness. A similar study for plane geometry was carried out in the work of Zhang [30]. Chen and colleagues [31] analyzed the different cross-sectional shape and inner surface angle of the FS and suggested the use of a rounded shape as intermediate between stepped and tapered. The results of numerical simulations and experiments have shown that changing the shape from conventional tapered (similar to Figure 3b) to concave (Figure 3c) can increase the magnetic field flux by ~10%, with virtually no loss in strength.

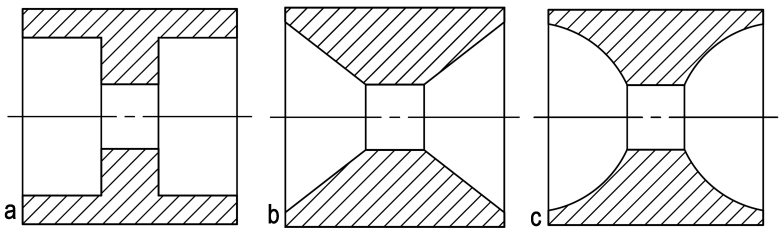

Figure 3. Schematic of different shapes of field-shaper cross-sections: stepped (**a**), tapered (**b**), concave (**c**)

 doi:10.20944/preprints202403.1582.v1

It should be noted that the use of FS is not necessary for the technology, however it has advantages: it is replaceable, so it increases the service life of the inductor, and different field-shapers may be used to fit workpieces of different sizes.

3. Experimental

3.1. Field-Shaper Design and Testing

In this work, we used 2x8 mm rectangular wire of a nanostructured Cu-Nb composite produced by (Rusatom MetalTech LLC., Moscow, Russia) [13]. Copper-niobium alloy wires (with 18% Nb) were cold drawn in a copper shell thus forming polygonal cross-section filaments, as can be seen in the Figure 4. The initial wire has the following characteristics: its resistivity is 2.8 μOhm*cm, yield strength is 860 MPa, tensile strength is 1260 MPa.

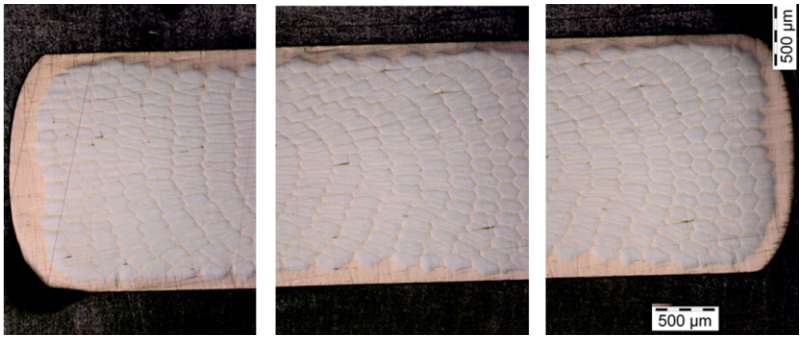

Figure 4. Cros-section of Cu-Nb rectangular wire (edges and central part)

The wire pieces were annealed in air atmosphere at 700°C for 8 min followed by cooling in water. After annealing, they were cold-deformed at room temperature with a punch and a die into $\Omega-$ and $W-$ shaped parts with a central angle of 180° for two-gap FS and 90° for four-gap FS (Figure 5a). The obtained parts from the Cu-Nb were brazed to the inner surface of 30KhGSA FS-body (Figure 5b) using PSr-40 hard solder (40% silver, 26% cadmium, 17% copper, 16.7% zinc, 0.3% nickel) with the direction of the fibers along the current lines (Figure 5c,d). After short-term annealing in air and brazing, the yield strength of the wire reduces to 515 MPa, the tensile strength to 890 MPa [32]. After the brazing the FS parts were milled and grinded to final dimensions: outer diameter 30 mm, length 30 mm; bore (channel) sizes: diameter is 9.5 mm and length is 12 mm, with 5 mm radius rounding of the transition to the coil working bore (Figure 6).

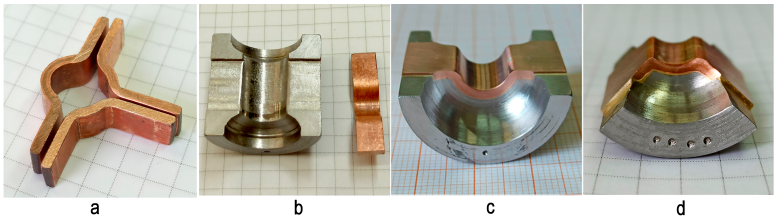

Figure 5. Parts of the field-shapers before (**a,b**) and after brazing, machining and grinding (**c,d**)

 doi:10.20944/preprints202403.1582.v1

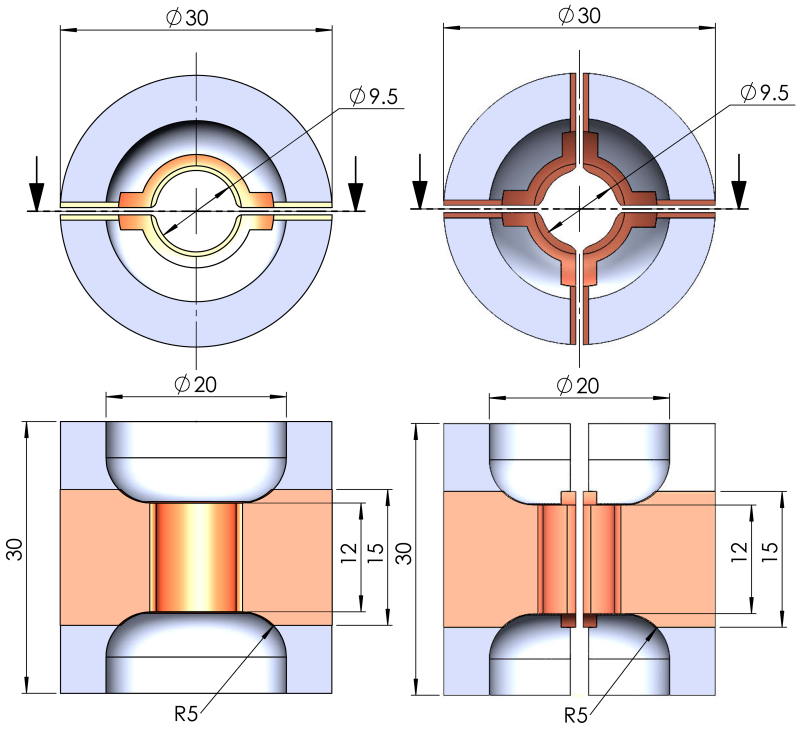

Figure 6. Constructions of FS

3.2. FEM Modelling of Magnetic Field Generation with Different Filed-Shapers

To determine the magnetic field distribution in the inductor system with FS of different types and validate experimental results, FEM calculations were performed with the Ansys Electronics Desktop 2021 R2 (Ansys ED) software package in the Maxwell 3D module. The current is given as a sine function of time:

$$I = I_0 \sin \frac{2\pi}{T} t, \tag{4}$$

where T is the period of electromagnetic (EM) field oscillations, it was taken equal to 28 μs (as in the experimental setup), the maximum current I_m was set so that the maximum magnetic field B_m was equal to 40 T. The calculations were performed in time until the first magnetic field maximum B_m at t = 7 μs. The time step in the calculation was 0.1 μs.

The sizes of the inductor and FS and the physical properties of their materials were the same in calculation and experiments. Resistivity values of 45, 1.72 and 2.8 μOhm*cm were measured by 4-probe DC method for 30KhGSA steel, copper and Cu-Nb composite respectively. The relative magnetic permeability of steel μ was assumed to be 1, since the calculation was performed for magnetic fields much higher than the magnetization limit of steels. Meshing was performed using built-in Ansys ED tools. 3 geometries were studied (A, B, C), the final mesh is shown in Figure 7, in each one the plate material was either Cu-Nb or 30KhGSA steel.

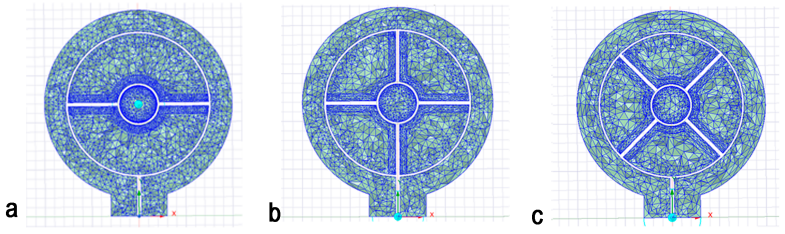

Figure 7. FS geometries studied: 2-slit FS (**a**), 4-slit FS with perpendicular slits with inductor (**b**), 4-slit FS with 45° slit angle (**c**)

 doi:10.20944/preprints202403.1582.v1

3.3. Experimental Study of Magnetic Field Generation

The manufactured system of inductor and FS has been tested under the generation of HMF with an amplitude of 40 T and a half-period duration of 14 μs (Figure 8). Pulsed current generator (PCG) with a capacitive-type storage device was used in this work (C = 425 μF, intrinsic inductance L_0 = 15 nH, intrinsic resistance R_0 = 1.5 mOhm, charging energy is up to 135 kJ). The generator supplies pulsed currents up to 2 MA to the inductor. These high currents in the discharge circuit were measured with a Rogowski coil, while the magnetic fields on the workpiece surface were measured with a pick-up coil (Figure 8b,c). In order to make repeated measurements, a rod of CuBe2, 8.55 mm in diameter, was inserted in the field-shaper instead of MPW workpieces. Beryllium bronze was chosen because of the combination of high conductivity, 6.5 μOhm*cm, and high yield strength, 600-950 MPa. A loop-shaped inductive magnetic field sensor (Figure 8,c) was installed axially in the middle of the inductor channel. It covered an area of 5 mm^2 of the magnetic flux Φ inside the inductor channel. The actual magnetic field in teslas was calculated by integrating the voltage from the sensor, which was recorded by an oscilloscope.

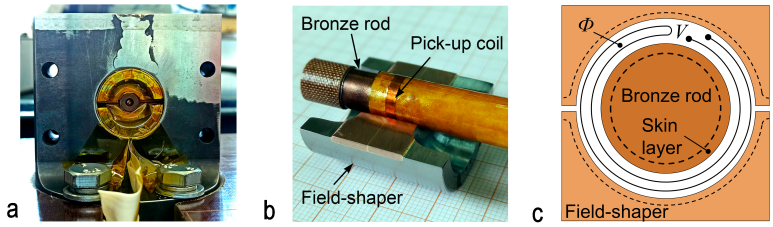

Figure 8. Field-shaper with magnetic field sensor inside the coil (**a**), the pick-up coil (**b**), schematic of the coil covering the bronze rod inside the field-shaper (**c**)

Magnetic field amplitudes in MPW experiments were calculated using B_m / I_m ratio from the above measurements taking into account the thickness of the skin layer in the materials of the field-shaper, bronze rod and copper driver, and heating effect of eddy currents on the conductivity of these parts. During the movement of the driver tube in MPW, the current through the parts and the magnetic field in the gap are redistributed, which may be the topic of a separate study, therefore, the field here was calculated under the assumption that the shell does not move.

3.4. Magnetic Pulse Tube Forming and Welding

The distributions of the magnetic field in the developed systems were characterized experimentally by compressing of empty tubes and performing magnetic pulse welding in the made field-shapers. The empty tubes of annealed copper (Cu-DHP) were 9.5 mm in outer diameter and 0.85 mm in wall thickness.

Finally, the joining of steel tubes to plugs has been performed using the developed field-shapers. The tubes and plugs were made of STS410 (an analog of AISI410), heat- and corrosion-resistant steel, often used in heat and hydraulic engineering. Its chemical composition is presented in Table 1. The tubes had an outer diameter of 7 mm and a wall thickness of 0.6 mm. The end plugs geometry is shown at Figure 9. A 0.5 mm thick copper driver was used to more efficiently transform the magnetic field energy into the kinetic energy of the steel tube.

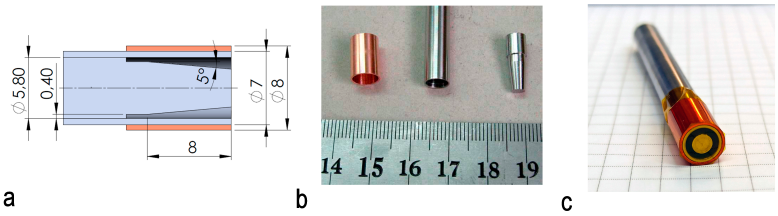

Figure 9. Joining geometry: tube, plug, and driver (**a**) and a picture of the parts (**b,c**)

 doi:10.20944/preprints202403.1582.v1

Table 1. Chemical composition of STS410 steel.

C	Si	Mn	Cr	Ni	Mo	Nb	V	W	Fe
0.15	0.49	0.55	11.96	0.18	0.1	0.01	0.04	0.02	bal.

To investigate the impact of magnetic field inhomogeneity on the quality of the welded joint, the parts were cut along the axis in the planes with the maximum and minimum field amplitudes.

4. Results and Discussion

4.1. FEM Analysis

FEM study of magnetic field generation processes in inductors with FS have shown the following results (Figure 10). The ratio of the magnetic field maxima in the cylindrical part of the gap between the FS and the inserted rod to the current in the primary inductor coil were: for the FS with a Cu-Nb plate: 61 T/MA in a two-slit FS and 54 T/MA in a four-slit FS for both installation angles. For the FS composed entirely of 30KhGSA steel this ratio was 51 and 42 T/MA respectively. The use of a Cu-Nb brazed plate instead of a whole-steel FS resulted in a significant increase in B_m / I_m of the inductor, by about 20% in the two slit and 29% in the four-slit FS, due to thinner skin layer in Cu-Nb compared to steel.

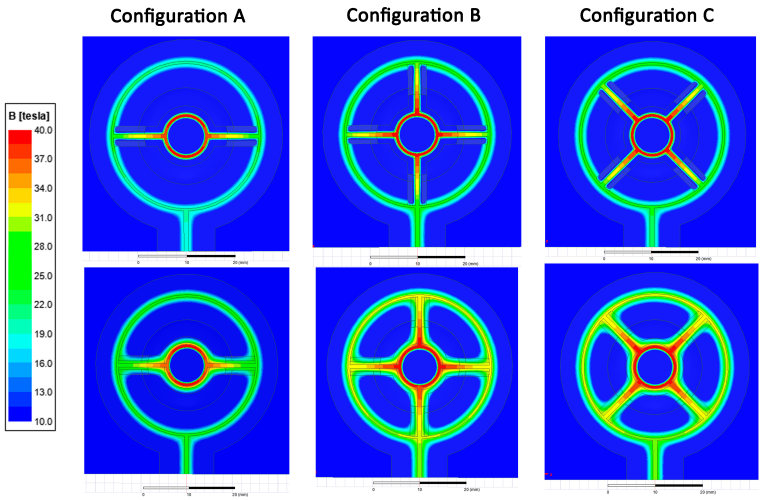

Figure 10. Field distribution in different inductor systems: Cu-18Nb plate in the top row on the FS surface, 30KhGSA plate in the bottom row.

The azimuthal distribution of the field in the gap is plotted along a line displaced by 0.2 mm from the surface of the copper rod to exclude the influence of mesh defects. (Figure 11). In configuration A, the largest field drops are observed at angles 0 and 180°, which corresponds to the gaps between the FS parts. The difference between the maximum and minimum field values in such a system with a copper-niobium plate is 6%. Replacing the plate with 30KhGSA steel leads to an even greater decrease - by 9%. Consequently, the magnetic field pressure ($P \sim B^2$), on the workpiece will decrease by 12 and 17%, respectively. Increasing the number of FS segments effects on the homogeneity of the magnetic field - regardless of the position of the gaps and even the material, the difference between the maximum and minimum field value will be about 3% which is 6% magnetic pressure difference. These results have shown that although the use of steel reduces the inductor efficiency, it is possible to obtain a sufficiently homogeneous field in a steel FS by increasing the number of its parts.

 doi:10.20944/preprints202403.1582.v1

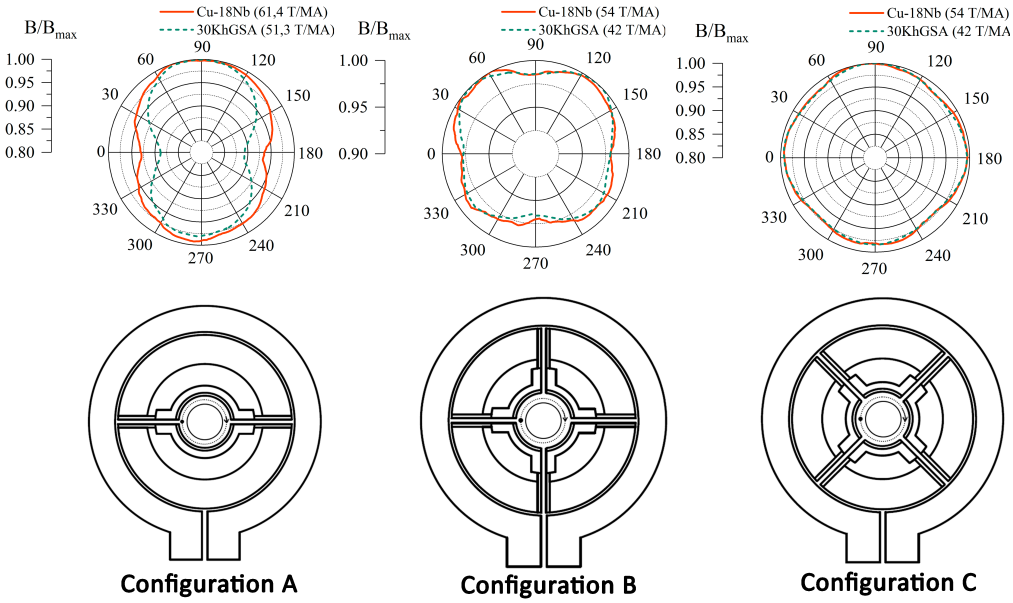

Figure 11. Azimuthal distribution of the magnetic field for different inductor system configurations

4.2. Magnetic Field Generation

The measured ratios of peak magnetic field to peak battery discharge current were 56.3 T/MA for 2-slit FS and 50.6 T/MA for 4-slit FS. This data was collected at 40 T peak magnetic field with the described above loop inductive sensor. The same technique we used in [33], which gave the ratio of 43 T/MA in a 30KhGSA steel 2-slit field-shaper. In the homogeneity experiment the compressed empty copper tubes after 48 T / 14 μs magnetic field pulse with their cross-sections are presented in the Figure 12.

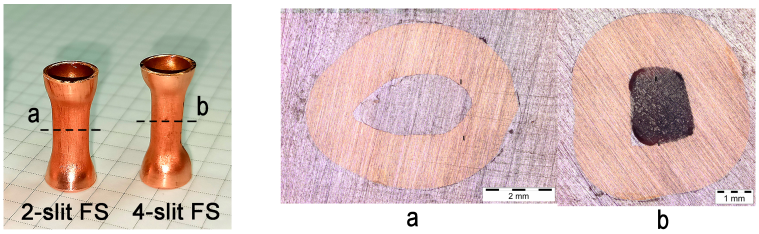

Figure 12. Deformed empty copper tubes after 48 T / 14 μs magnetic field pulse

To describe the azimuthal homogeneity of magnetic field pressure applied to the copper tube we used uniformity coefficient η, calculated values presented in Table 2:

$$\eta = \frac{D_{max} - D_{min}}{D_{max}} \cdot 100\%, \tag{5}$$

where D_{max} is the maximum diameter and D_{min} is the minimum diameter of the deformation center (Figure 13).

Table 2. Characteristics of comressed Cu tube.

	D_0	D_{min}	D_{max}	η, %
2-slit FS	9.55	4.9	6.7	27
4-slit FS	9.55	5.2	5.7	7

 doi:10.20944/preprints202403.1582.v1

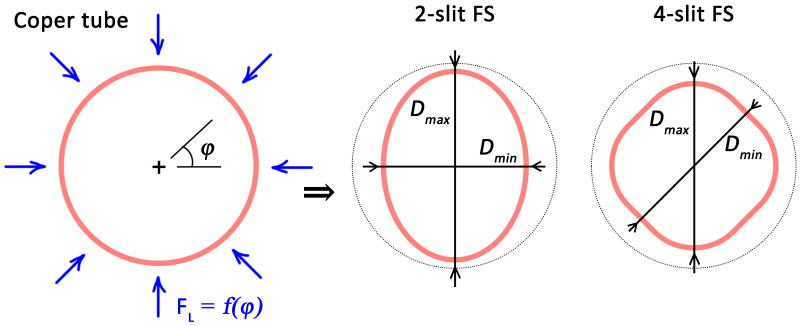

Figure 13. Tube profile schematic before and after compression

4.3. MPW Experiment

The ends of the samples after MPW retained the imprint of the field-shaper in which they were welded (Figure 14).

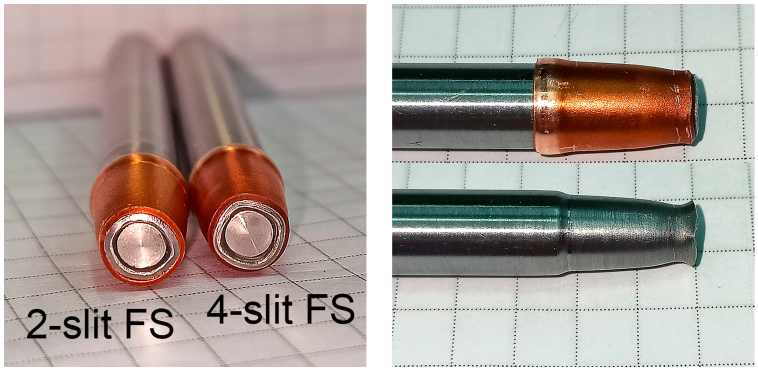

Figure 14. Samples after MPW before and after Cu-driver peeling

Cut, grinded, and polished samples were studied by optical microscopy with an Olympus BX41M microscope. The cut planes are shown in Figure 15. Plane 1 coincided with the inductor slit, plane 2 is rotated at 90° to plane 1 for the 2-slit FS, and at 45° to plane 1 for the 4-slit FS. Each image in Figure 16 displays a cut of one sample in these two planes, plane 1 for the top specimen, and plane 2 for the bottom specimen. Under the microscopic examination, the weld appears as a fusion of the pipe and plug. A discernible dark line indicates a gap between the parts, or the area where they are not welded. The fusion length L_1 and L_2 of the weld joint in the high and low field amplitude areas was visually determined and summarized in Table 3. The lengths of the welded joint are close to each other in planes 1 and 2 of higher and lower magnetic pressure, which indicates good circumferential symmetry of MPW in these field-shapers. The torn-off ends of the plugs indicate a slightly excessive magnetic pressure during MPW, however, this did not affect the symmetry of the processed samples.

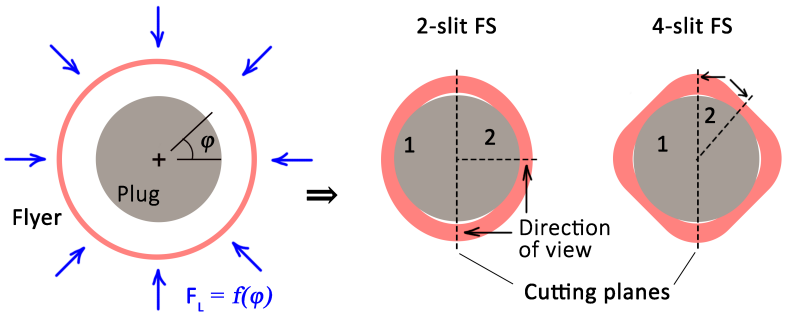

Figure 15. Scheme of sample preparation after MPW

 doi:10.20944/preprints202403.1582.v1

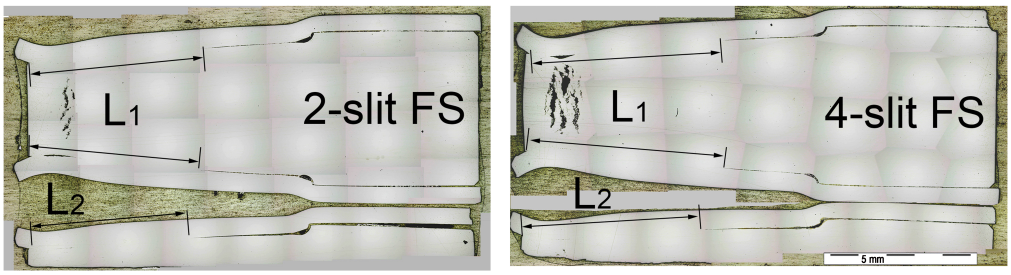

Figure 16. Optical microscopy of welded samples in different FS: (a) two-slit FS, (b) four-slit FS

In previous work, we joined STS410 steel parts in an all-steel single-turn inductor without a field-shaper [34]. In comparison to average joining length between the samples welded at 8.5 kV in [34] the samples in the present work are more symmetrical with 4-slit field-shaper, which can be seen from weld lengths relative difference in Table 3.

Table 3. MPW parameters and the length of welded joining.

	U_0, kV	I_m, kA	B_m, T	$<L_1>$,mm	L_2,mm	Rel. diff., %
2-slit Cu-Nb	10.7	828	45	5.38	6.02	11
4-slit Cu-Nb	12	950	46	6.46	6.37	1.4
1-slit Steel coil	8.5	705	40	6.64	5.66	16

5. Conclusions

In the present work, a new approach has been attempted to use nanostructured Cu-18%Nb composite wire in field-shapers for high pulsed magnetic field of microsecond duration. FEM modeling of the field distribution was performed, as well as field generation experiments with an amplitude up to 48 T, and a half-period of 14 μs. The considered inductor systems have a number of advantages over the most common steel and bronze ones:

1. The use of composite Cu-Nb wire leads to improved energy efficiency of the inductor system: the field-to-current maximum ratios were 56.3 T/MA for 2-slit FS and 50.6 T/MA for 4-slit FS, which are 31 and 18% higher, respectively, compared to 43 T/MA of a whole steel FS. Experimental values were confirmed by FEM analysis.
2. In comparison with bronze field-shapers, the Cu-Nb ones have higher lifetime, being able to withstand at least tens of 50 T magnetic field pulses, whereas the bronze ones have considerable thermal cracking after 5-10 pulses of 50T magnetic field.
3. The use of highly-conductive composite material improves magnetic field homogeneity in azimuthal direction inside the working channel of the 2-slit FS: the difference between the maximum and minimum field value is 6% for composite FS versus 9% for steel FS (FEM).
4. Magnetic pulse welding of a stainless STS410 steel tube and plug was performed using the new FS. Examination of the welds in the areas of maximum and minimum field amplitude indicated a high level of azimuthal homogeneity of the obtained joints. The relative difference in weld lengths is 11% mm for 2-slit FS and 1.4% for 4-slit FS. This is higher than 16% for the steel coil presented in the previous works.

Author Contributions: The study conception and design were performed by Vasiliy Krutikov, Spirin Alexey and Sergey Paranin. Development of inductor system and experimental work were performed by Vasiliy Krutikov.

FEM analysis was performed by Evgeny Zaytsev. Sample preparation, data analysis, including literature review, figure and schemes preparation by Vasiliy Krutikov and Evgeny Zaytsev. Original draft preparation by Evgeny Zaytsev. Supervision, project administration, funding acquisition by Vasiliy Krutikov. All authors read and approved the final manuscript.

Funding: This research was funded by the Russian Science Foundation (RSF) under Grant No. 22-79-00307, https://rscf.ru/en/project/22-79-00307/.

Data Availability Statement: The data presented in this study are available on request from the corresponding author.

Acknowledgments: The studies were carried out using the equipment of the common use center "Electrophysics" on the basis of the Institute of Electrophysics of the Ural Branch of the Russian Academy of Sciences.

Conflicts of Interest: The authors declare no conflicts of interest.

References

1. Kapil, A.; Sharma, A. Magnetic pulse welding: an efficient and environmentally friendly multi-material joining technique. *Journal of Cleaner Production* **2015**, *100*, 35–58. https://doi.org/10.1016/j.jclepro.2015.03.042.
2. Krutikov, V.; Paranin, S.; Spirin, A.; Kazakov, A.; Aleksandrov, E. Fabrication of thin-walled iridium tubular articles by radial magnetic pulsed compaction and sintering of nanopowder. *Letters on Materials* **2019**, *9*, 334–338. https://doi.org/10.22226/2410-3535-2019-3-334-338.
3. McGinley, J. Electromagnetic Pulse Technology as a Means of Joining Generation IV Cladding Materials. In Proceedings of the Volume 1: Plant Operations, Maintenance, Engineering, Modifications and Life Cycle; Component Reliability and Materials Issues; Next Generation Systems. ASMEDC, 1 2009, ICONE17. https://doi.org/10.1115/icone17-75630.
4. Lee, J.G.; Park, J.J.; Lee, M.K.; Rhee, C.K.; Kim, T.K.; Spirin, A.; Krutikov, V.; Paranin, S. End Closure Joining of Ferritic-Martensitic and Oxide-Dispersion Strengthened Steel Cladding Tubes by Magnetic Pulse Welding. *Metallurgical and Materials Transactions A* **2015**, *46*, 3132–3139. https://doi.org/10.1007/s11661-015-2905-5.
5. Song, J.W.; Park, J.J.; Lee, G.J.; Lee, M.K.; Park, K.H.; Hong, S.J.; Lee, J.G. Effect of Impact Velocity on Interface Characteristics of HT-9 Steel Joints Fabricated by Magnetic Pulse Welding. *Metals and Materials International* **2019**, *26*, 360–369. https://doi.org/10.1007/s12540-019-00510-0.
6. Kulkarni, M.R.; Kolge, T.; Kumar, D.; Kore, S.D.; Sharma, A.; Srikanth, V.; Laik, A.; Chakraborty, G.; Albert, S. Magnetic Pulse Welding of D9 Steel Tube to SS316LN End Plug. *Transactions of the Indian Institute of Metals* **2022**, *75*, 171–182. https://doi.org/10.1007/s12666-021-02413-4.
7. Sharma, S.K.; JMMVS, A.; Mishra, S.; Rani, R.; Mishra, S.; Waghmare, N.; Sharma, A. Generation of 0.5 to 0.6 Mega Gauss Pulse Magnetic Field for Magnetic Pulse Welding of High Strength Alloys. In Proceedings of the 2018 16th International Conference on Megagauss Magnetic Field Generation and Related Topics (MEGAGAUSS), 2018, pp. 1–4. https://doi.org/10.1109/MEGAGAUSS.2018.8722676.
8. Adamyan, Y.E.; Alekseev, D.I.; Chernenkaya, L.V.; Krivosheev, S.I.; Magazinov, S.G.; Titkov, V.V. Interaction the high-density pulse current with material in the zone of local conduction disturbance at the edge of a thin wall magnetic system. In Proceedings of the 2018 16th International Conference on Megagauss Magnetic Field Generation and Related Topics (MEGAGAUSS), 2018, pp. 1–4. https://doi.org/10.1109/MEGAGAUSS.2018.8722688.
9. Shneerson, G.A.; Dolotenko, M.I.; Krivosheev, S.I. *Strong and Superstrong Pulsed Magnetic Fields Generation*; De Gruyter: Berlin, München, Boston, 2014. https://doi.org/doi:10.1515/9783110252576.
10. Furth, H.P.; Levine, M.A.; Waniek, R.W. Production and Use of High Transient Magnetic Fields. II. *Review of Scientific Instruments* **1957**, *28*, 949–958. https://doi.org/10.1063/1.1715773.
11. Han, K.; Toplosky, V.; Walsh, R.; Swenson, C.; Lesch, B.; Pantsyrnyi, V. Properties of high strength Cu-Nb conductor for pulsed magnet applications. *IEEE Transactions on Applied Superconductivity* **2002**, *12*, 1176–1180. https://doi.org/10.1109/TASC.2002.1018611.
12. Bevk, J.; Harbison, J.P.; Bell, J.L. Anomalous increase in strength of in situ formed Cu-Nb multifilamentary composites. *Journal of Applied Physics* **1978**, *49*, 6031–6038. https://doi.org/10.1063/1.324573.
13. Shikov, A.K.; Pantsyrnyi, V.I.; Vorob'eva, A.E.; Sud'ev, S.V.; Khlebova, N.E.; Silaev, A.K.; Belyakov, N.A. Copper-Niobium High-Strength and High-Conductivity Winding Wires for Pulsed Magnets. *Metal Science and Heat Treatment* **2002**, *44*, 491–495. https://doi.org/10.1023/a:1022504805662.

14. Heringhaus, F.; Raabe, D.; Gottstein, G. On the correlation of microstructure and electromagnetic properties of heavily cold worked Cu-20 wt*Acta Metallurgica et Materialia* **1995**, *43*, 1467–1476.
15. Reza Toroghinejad, M.; Ashrafizadeh, F.; Jamaati, R. On the use of accumulative roll bonding process to develop nanostructured aluminum alloy 5083. *Materials Science and Engineering: A* **2013**, *561*, 145–151. https://doi.org/10.1016/j.msea.2012.11.010.
16. Novickij, J.; Višniakov, N. The Application of Composite Materials in Pulsed Inductor Design. In Proceedings of the Mechatronic Systems and Materials. Trans Tech Publications Ltd, 7 2006, Vol. 113, *Solid State Phenomena*, pp. 545–548. https://doi.org/10.4028/www.scientific.net/SSP.113.545.
17. Lagutin, A.; Rosseel, K.; Herlach, F.; Vanacken, J.; Bruynseraede, Y. Development of reliable 70 T pulsed magnets. *Measurement Science and Technology* **2003**, *14*, 2144. https://doi.org/10.1088/0957-0233/14/12/015.
18. Peng, T.; Jiang, F.; Sun, Q.Q.; Xu, Q.; Xiao, H.X.; Herlach, F.; Li, L. Design and Test of a 90-T Nondestructive Magnet at the Wuhan National High Magnetic Field Center. *IEEE Transactions on Applied Superconductivity* **2014**, *24*, 1–4. https://doi.org/10.1109/TASC.2013.2284273.
19. Zherlitsyn, S.; Bianchi, A.; Herrmannsdoerfer, T.; Pobell, F.; Skourski, Y.; Sytcheva, A.; Zvyagin, S.; Wosnitza, J. Coil Design for Non-Destructive Pulsed-Field Magnets Targeting 100 T. *IEEE Transactions on Applied Superconductivity* **2006**, *16*, 1660–1663. https://doi.org/10.1109/TASC.2005.864297.
20. Peng, T.; Jiang, F.; Sun, Q.Q.; Pan, Y.; Herlach, F.; Li, L. Concept Design of 100-T Pulsed Magnet at the Wuhan National High Magnetic Field Center. *IEEE Transactions on Applied Superconductivity* **2016**, *26*, 1–4. https://doi.org/10.1109/TASC.2015.2513366.
21. Peng, T.e.a. A Novel Design of Multi-Coil Pulsed Magnet System for 100 T. *IEEE Transactions on Applied Superconductivity* **2022**, *32*, 1–4. https://doi.org/10.1109/TASC.2022.3148049.
22. Wittman, R. The influence of collision parameters of the strength and microstructure of an explosion welded aluminium alloy., 1973. In Proceedings of the Proc. 2nd Int. Sym. on Use of an Explosive Energy in Manufacturing Metallic Materials, Marianske Lazne, Czech Republic, 9-12 October 1973.
23. Deribas, A. *Fizika uprochneniya i svarki vzrivom*; Nauka: Novosibirsk, Russia, 1980.
24. Ribeiro, J.B.; Mendes, R.; Loureiro, A. Review of the weldability window concept and equations for explosive welding. *Journal of Physics: Conference Series* **2014**, *500*, 052038. https://doi.org/10.1088/1742-6596/500/5/052038.
25. Yan, Z.; Lin, L.; Chen, Y.; Cui, X.; ping Ye, S.; Qiu, D.; Zhang, L. Electromagnetic flanging using a field shaper with multiple seams. *The International Journal of Advanced Manufacturing Technology* **2022**, *120*, 1747 – 1763. https://doi.org/10.1007/s00170-022-08842-9.
26. Yan, Z.; Xiao, A.; Cui, X.; Guo, Y.; Lin, Y.; Zhang, L.; Zhao, P. Magnetic pulse welding of aluminum to steel tubes using a field-shaper with multiple seams. *Journal of Manufacturing Processes* **2021**, *65*, 214–227. https://doi.org/10.1016/j.jmapro.2021.03.037.
27. Shen, T.; Li, C.; Zhou, Y.; Wu, H.; Wang, X.; Xu, Q. The effect of assembly of coil and field shaper on electromagnetic pulse crimping. *Energy Reports* **2022**, *8*, 1243–1248. 2021 The 8th International Conference on Power and Energy Systems Engineering, https://doi.org/10.1016/j.egyr.2021.11.213.
28. Rajak, A.K.; Kumar, R.; Basumatary, H.; Kore, S.D. Numerical and Experimental Study on Effect of Different Types of Field-Shaper on Electromagnetic Terminal-Wire Crimping Process. *International Journal of Precision Engineering and Manufacturing* **2018**, *19*, 453–459. https://doi.org/10.1007/s12541-018-0055-6.
29. Rajak, A.K.; Kumar, R.; Kore, S.D. Designing of field shaper for the electro-magnetic crimping process. *Journal of Mechanical Science and Technology* **2019**, *33*, 5407–5413. https://doi.org/10.1007/s12206-019-1035-1.
30. Zhang, H.; Liu, N.; Li, X.; Deng, F.; Wang, Qingji andDing, H. A novel field shaper with slow-varying central hole for electromagnetic pulse welding of sheet metal. *The International Journal of Advanced Manufacturing Technology* **2020**, *108*, 2595–2606. https://doi.org/10.1007/s00170-020-05454-z.
31. Chen, Y.; Yang, Z.; Peng, W.; Zhang, H. Experimental investigation and optimization on field shaper structure parameters in magnetic pulse welding. *Proceedings of the Institution of Mechanical Engineers, Part B: Journal of Engineering Manufacture* **2021**, *235*, 2108–2117. https://doi.org/10.1177/09544054211014846.
32. Zaytsev, E.; Spirin, A.; Krutikov, V.; Paranin, S.; Zayats, S.; Kaigorodov, A.; Koleukh, D.; Kebets, A. Development of material based on nanostructured Cu-Nb alloy for high magnetic field coils of microsecond duration. In Proceedings of the 8th International Congress on Energy Fluxes and Radiation Effects. Crossref, 11 2022, EFRE-2022. https://doi.org/10.56761/efre2022.s4-o-038401.

 doi:10.20944/preprints202403.1582.v1

33. Spirin, A.V.; Krutikov, V.I.; Koleukh, D.S.; Mamaev, A.S.; Paranin, S.N.; Gavrilov, N.V.; Kaigorodov, A.S. Effect of structural steel ion plasma nitriding on material durability in pulsed high magnetic fields. *Journal of Physics: Conference Series* **2017**, *830*, 012080. https://doi.org/10.1088/1742-6596/830/1/012080.
34. Krutikov, V.; Paranin, S.; Ivanov, V.; Spirin, A.; Koleukh, D.; Lee, J.G.; Lee, M.K.; Rhee, C.K. Magnetic Pulse Welding of the "Tube – Plug" Pair of STS410 Steel. In Proceedings of the 6th International Conference on High Speed Forming, March 27th-29th 2014, Daejeon, Korea, 2014, pp. 207–214. https://doi.org/10.17877/DE290R-855.